

From massive spirals to dwarf irregulars: a new set of tight scaling relations for cold gas and stars driven by disc gravitational instability

Alessandro B. Romeo^{1*}

¹*Department of Space, Earth and Environment, Chalmers University of Technology, SE-41296 Gothenburg, Sweden*

Accepted 2019 November 28. Received 2019 November 25; in original form 2019 May 14

ABSTRACT

We present a new set of galaxy scaling relations for the relative mass content of atomic gas, molecular gas and stars. Such relations are driven by disc gravitational instability, and originate from the low galaxy-to-galaxy variance of Toomre’s Q stability parameter. We test such relations using more than 100 galaxies, from massive spirals to dwarf irregulars, thus spanning several orders of magnitude in stellar mass ($M_{\star} \approx 10^{6-11} M_{\odot}$) and atomic gas mass ($M_{\text{HI}} \approx 10^{7-10.5} M_{\odot}$). Such tests demonstrate (i) that our scaling relations are physically motivated and tightly constrained, (ii) that the mass-averaged gravitational instability properties of galaxy discs are remarkably uniform across the sequence Sa–dIrr, and (iii) that specific angular momentum plays an important role in such a scenario. Besides providing new insights into a very important topic in galaxy evolution, this work provides a simple formula (Eq. 5) that one can use for generating other galaxy relations driven by disc instability. We explain how to do that, mention a few possible applications, and stress the importance of testing our approach further.

Key words: instabilities – stars: kinematics and dynamics – ISM: kinematics and dynamics – galaxies: ISM – galaxies: kinematics and dynamics – galaxies: star formation.

1 INTRODUCTION

Statistical correlations between physical properties of galaxies are indispensable tools for unravelling the fundamental laws that govern galaxy formation and evolution across the observed variety of scales. Such ‘scaling relations’ are therefore constantly used for testing simulation and semi-analytic models of galaxy evolution, and for constraining their predictions (e.g., Dutton et al. 2011; Lagos et al. 2016; Agertz et al. 2019; Forbes et al. 2019; Ginolfi et al. 2019). Discovering new scaling relations is thus very important, and so is determining the physical processes that drive them.

Recent examples of galaxy scaling relations that have attracted special interest are those linking the relative mass content of atomic and molecular gas to stellar mass, or to related properties like stellar mass surface density, specific star formation rate and colour (e.g., Saintonge et al. 2011; Huang et al. 2012; Boselli et al. 2014; Catinella et al. 2018). Recent investigations focusing on spiral galaxies suggest that the atomic gas scaling relation is driven by disc gravitational instability. Obreschkow et al. (2016) proposed a hybrid stability model that predicts the mass fraction of atomic (hy-

drogen+helium) gas as a function of mass and specific angular momentum of the whole (gas+stars) disc via a newly defined q parameter, assuming a constant HI velocity dispersion ($\sigma_{\text{HI}} = 10 \text{ km s}^{-1}$). Such a stability model has been tested in a variety of applications, and found to be a reliable atomic gas tracer (e.g., Lagos et al. 2017; Lutz et al. 2017, 2018; Stevens et al. 2018; Wang et al. 2018; Džudžar et al. 2019; Murugesan et al. 2019; Stevens et al. 2019). Another important contribution is the one by Zasov & Zaitseva (2017), who showed that the relation between atomic gas mass and disc specific angular momentum is equally well described by a simpler stability model controlled by Q_{gas} , the gas Toomre parameter, assuming that Q_{gas} is approximately constant within a galaxy (like σ_{gas}). This stability model was tested and constrained by Kurapati et al. (2018).

The above-mentioned link between disc gravitational instability and disc angular momentum is another important aspect of the problem and has been investigated in many other works, not only in the original context of instability to bar formation (e.g., Mo et al. 1998; Athanassoula 2008; Agertz & Kravtsov 2016; Sellwood 2016; Okamura et al. 2018; Romeo & Mogotsi 2018; Zoldan et al. 2018; Valencia-Enríquez et al. 2019) but also in the context of Toomre instability, both at low z (e.g., Obreschkow & Glazebrook 2014;

* E-mail: romeo@chalmers.se

Stevens et al. 2016; Romeo & Mogotsi 2018) and at high z (e.g., Obreschkow et al. 2015; Stevens et al. 2016; Swinbank et al. 2017; Sweet et al. 2019). All such works find that there is a measurable link between disc gravitational instability and galactic angular momentum, but the resulting relation depends on which stability diagnostic is used.

Romeo & Mogotsi (2018) pointed out that Q_{gas} and q (Obreschkow et al. 2016) are not fully reliable stability diagnostics. This concerns not only nearby spirals, where stars are the primary driver of disc instabilities (Romeo & Fathi 2016; Romeo & Mogotsi 2017), but also gas-rich galaxies at high z and their nearby analogues, where turbulence can drive the disc into regimes that are far from Toomre/Jeans instability (Romeo et al. 2010; Romeo & Agertz 2014; see also Renaud 2019). Romeo & Mogotsi (2018) showed that a more reliable stability diagnostic for spiral galaxies is $\langle Q_{\star} \rangle$, the mass-weighted average of the stellar Toomre parameter, corrected so as to include disc thickness effects (Romeo & Falstad 2013). Such a diagnostic allowed them to tightly constrain the relation between stellar mass, stellar specific angular momentum and disc stability level. Romeo & Mogotsi (2018) also showed that $\langle Q_{\star} \rangle$ is related to the Efstathiou-Lake-Negroponte (1982) global stability parameter, ϵ_{m} , via the degree of rotational support, V/σ , and the velocity dispersion anisotropy, σ_z/σ_R . These are two important effects that are missing from ϵ_{m} .

This paper proposes a unified approach to the problem, which results in a new set of scaling relations for the relative mass content of cold gas and stars, and which is able to generate further useful scaling relations, all driven by disc gravitational instability. Unlike the models of Obreschkow et al. (2016) and Zasov & Zaitseva (2017), our approach does not assume that σ_{gas} or Q_{gas} is approximately constant within a galaxy, and applies not only to atomic gas but also to molecular gas and stars. While the present approach builds on the analyses performed by Romeo & Mogotsi (2017, 2018), the applications presented here are entirely new and concern disc-dominated galaxies of all morphological types (Sa–dIrr), thus spanning several orders of magnitude in stellar mass ($M_{\star} \approx 10^{6-11} M_{\odot}$) and atomic gas mass ($M_{\text{HI}} \approx 10^{7-10.5} M_{\odot}$). Our approach is presented in Sect. 2, where we show the route that connects Toomre’s Q stability parameter to our new set of scaling relations, and beyond. Galaxy samples, data and statistics are described in Sect. 3, the new set of scaling relations is presented and tested in Sect. 4, and the conclusions are drawn in Sect. 5.

2 A UNIFIED APPROACH FOR COLD GAS AND STARS

2.1 Choice of a representative galaxy sample and basic quantities

As a representative galaxy sample, we choose the popular sample of spirals originally selected and analysed by Leroy et al. (2008), hereafter L08: NGC 628, 2841, 3184, 3198, 3351, 3521, 3627, 4736, 5055, 5194, 6946 and 7331. These are 12 nearby star-forming galaxies with sensitive and spatially resolved measurements of atomic gas, molecular gas and stellar properties across the entire optical disc, compiled by combining data from several surveys. We refer to L08 for

a detailed description of the data and their translation into physical quantities (see their sect. 3).

L08’s sample of spirals provides all the quantities needed to carry out our analysis. In particular, among other quantities specified in Sect. 2.2, we use the same epicyclic frequency (κ), mass surface densities of atomic gas (Σ_{HI}), molecular gas (Σ_{H_2}) and stars (Σ_{\star}), and stellar radial velocity dispersion (σ_{\star}) as in L08 (see their appendices A–C and E–F). However, rather than using observationally motivated values of the H I and H₂ velocity dispersions, we use observed radial profiles of σ_{HI} and σ_{H_2} , which rise towards the centre in most of the galaxies (Romeo & Mogotsi 2017; see their sect. 2.1, and figs 1 and 2). Note also that the radial profiles of σ_{\star} derived by L08 are not based on observations, but on a simple model that relates σ_{\star} to the mass surface density and scale length of the stellar disc (see their appendix B.3). To the best of our knowledge, stellar velocity dispersions have only been measured in three galaxies of the sample: NGC 628 (Ganda et al. 2006; Herrmann & Ciardullo 2009), NGC 3198 (Bottema 1988, 1993) and NGC 4736 (Herrmann & Ciardullo 2009). However, L08’s model is quite reliable. Systematic uncertainties in σ_{\star} are significant, on average, only in the innermost/outermost regions of the stellar disc, where this model overestimates/underestimates the observed σ_{\star} (Romeo & Mogotsi 2017; Mogotsi & Romeo 2019). Those regions, however, have little weight in the present analysis.

2.2 Tour through disc gravitational instability

To explore the link between disc gravitational instability and the relative mass content of atomic gas, molecular gas and stars in galaxies, we start from the simplest stability diagnostic: the Toomre (1964) parameter, $Q = \kappa\sigma/\pi G\Sigma$. It is commonly assumed that $Q \approx 1$, consistent with a process of self-regulation that keeps galaxy discs close to marginal stability (see sect. 1 of Krumholz et al. 2018 for an overview). How realistic is that assumption? Fig. 1 illustrates that atomic gas, molecular gas and stars have distinct radial distributions of Q , which differ both in median trend and in variance. While Q_{\star} is quite close to unity, Q_{H_2} is three times more offset and scattered, whereas Q_{HI} exhibits a two-orders-of-magnitude decline within the optical radius and an even larger median offset from unity than Q_{H_2} . Thus the assumption that $Q \approx 1$ is not realistic enough to represent the diverse phenomenology of Q in galaxy discs.

Such a diversity results from the complex interplay between the heating and cooling processes that regulate the value of Q in galaxy discs (Krumholz & Burkert 2010; Forbes et al. 2012, 2014, 2019), and from the fact that Q_{HI} , Q_{H_2} and Q_{\star} do not really measure the stability levels of atomic gas, molecular gas and stars. Q_{HI} , Q_{H_2} and Q_{\star} are instead the building blocks of a more realistic, multi-component Q stability parameter (Romeo & Falstad 2013). Such a parameter is dominated by Q_{\star} because stars, and not molecular or atomic gas, are the primary driver of disc instabilities in spiral galaxies (Romeo & Mogotsi 2017; Marchuk 2018; Marchuk & Sotnikova 2018; Mogotsi & Romeo 2019), which is true even for a powerful starburst+Seyfert galaxy like NGC 1068 (Romeo & Fathi 2016). This is the reason why Q_{\star} is much closer to the critical stability level ($Q_{\text{crit}} \approx 2-3$) than Q_{H_2} or Q_{HI} . Note that Q_{crit} is higher than unity, but its precise value is still questioned (Romeo & Fathi 2015).

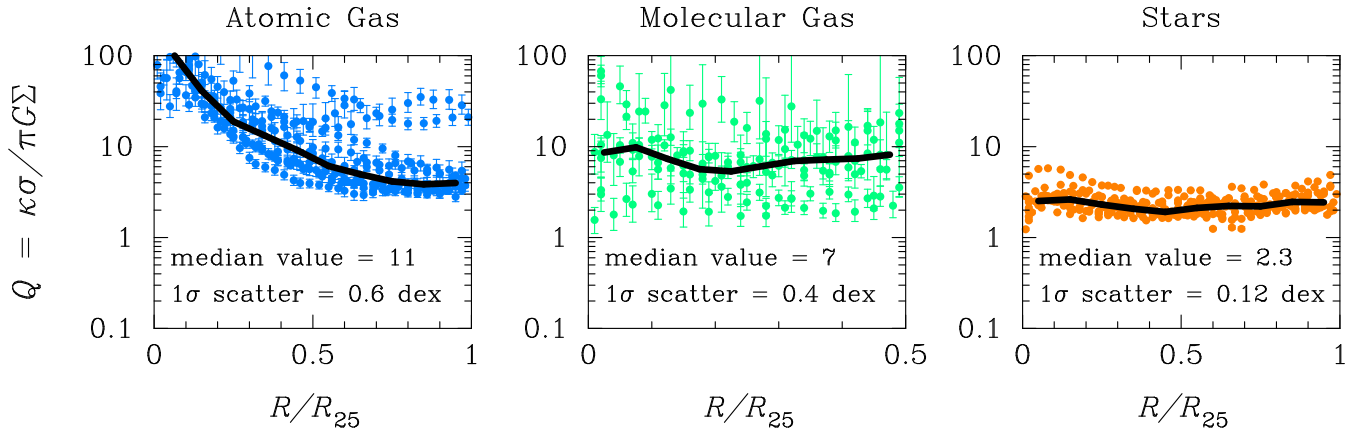


Figure 1. Radial profiles of the Toomre parameter for L08’s sample of spirals, with the galactocentric distance measured in units of the optical radius (B-band isophotal radius at 25 mag arcsec⁻²). Also shown is the local median of Q . In the case of molecular gas, the radial range is limited by the sparsity of sensitive CO measurements beyond half the optical radius.

In fact, Q_{crit} is influenced by complex phenomena such as non-axisymmetric perturbations (e.g., Griv & Gedalin 2012) and gas dissipation (Elmegreen 2011), whose effects are difficult to quantify. Disc thickness effects are instead easier to evaluate, and are already included in the definition of Q (see again Romeo & Falstad 2013).

Now that we have clarified how self-regulated galaxy discs are, let us analyse how the Toomre parameter of component i , $Q_i = \kappa\sigma_i/\pi G\Sigma_i$, varies from galaxy to galaxy. To suppress the variation of Q_i within a galaxy, we take the mass-weighted average of $Q_i(R)$:

$$\langle Q_i \rangle = \frac{1}{M_i(R_{\text{av}})} \int_0^{R_{\text{av}}} Q_i(R) \Sigma_i(R) 2\pi R dR. \quad (1)$$

This type of average is especially useful because it relates $\langle Q_i \rangle$ to fundamental galaxy properties such as mass, M_i , and specific angular momentum, $j_i = J_i/M_i$, via a simple and accurate approximation (Romeo & Mogotsi 2018). The resulting relation is $\langle Q_i \rangle \propto \mathcal{A}_i$, where

$$\mathcal{A}_i = \frac{j_i \bar{\sigma}_i}{GM_i}, \quad (2)$$

$$j_i = \frac{1}{M_i} \int_0^\infty R v_c(R) \Sigma_i(R) 2\pi R dR, \quad (3)$$

$$\bar{\sigma}_i = \frac{1}{R_{\text{av}}} \int_0^{R_{\text{av}}} \sigma_i(R) dR. \quad (4)$$

Note four points concerning Eqs (1)–(4):

- M_i and j_i are the total mass and the total specific angular momentum of atomic hydrogen+helium gas ($i = \text{H1}$), molecular hydrogen+helium gas ($i = \text{H2}$) or stars ($i = \star$).

- Our definition of j_i is based on that of Obreschkow & Glazebrook (2014), and assumes that stars and gas follow exactly the same rotation curve. This is technically not correct and tends to overestimate j_\star (El-Badry et al. 2018; Fall & Romanowsky 2018; Posti et al. 2018a) because it neglects asymmetric drift corrections, which are significant where $\sigma_\star \gtrsim v_c$ (see, e.g., Binney & Tremaine 2008). However, our definition of j_i is the one most commonly used for precision measurement of angular momentum in disc galaxies (e.g., Obreschkow & Glazebrook 2014; Butler et al. 2017; Chowd-

hury & Chengalur 2017; Elson 2017; Kurapati et al. 2018). More importantly, our definition of j_i is fully consistent with the epicyclic approximation, $\sigma_i/R\kappa \ll 1$ (hence $\sigma_i \ll v_c$), a fundamental assumption behind Toomre’s stability criterion and its descendants (see, e.g., Bertin 2014).

- While $\langle Q_i \rangle$ is the mass-weighted average of $Q_i(R)$, $\bar{\sigma}_i$ is the radial average of $\sigma_i(R)$, where σ denotes the radial velocity dispersion.

- \mathcal{A}_i may look identical to the q parameter defined by Obreschkow et al. (2016), but it is not. For instance, \mathcal{A}_i applies not only to atomic gas but also to molecular gas and stars, and does not assume that σ_i is constant. As pointed out in Sect. 1, our approach is also significantly different from the Obreschkow et al. (2016) model, and so are the resulting scaling relations, as we will show in Sect. 4.2.

Last but not least, note that the coefficient of proportionality between $\langle Q_i \rangle$ and \mathcal{A}_i is a numerical factor that depends on R_{av}/l_i , where R_{av} is the radius over which $Q_i(R)$ is averaged (see Eq. 1) and l_i is the exponential scale length of component i . So this factor is not well defined for a component whose mass distribution is far from exponential, like atomic gas (e.g., Bigiel & Blitz 2012). In view of that, we opt for a unified approach and use \mathcal{A}_i as a proxy for $\langle Q_i \rangle$: it is well defined for all the components, and it is simpler than $\langle Q_i \rangle$. In addition, the offset of \mathcal{A}_i from $\langle Q_i \rangle$ is not an issue because $Q_i = 1$ no longer means marginal stability when the disc has multiple, gravitationally coupled components (Romeo & Falstad 2013; see also Fig. 1 and its discussion), and because any such numerical factor will be statistically suppressed by the final rescaling made in Sect. 2.3. This is also the reason why we have not corrected Q_i so as to include disc thickness effects.

To compute the \mathcal{A}_i stability parameter for L08’s sample of spirals, we use the values of M_i and j_i tabulated by L08 and Obreschkow & Glazebrook (2014), respectively. We also need to evaluate $\bar{\sigma}_i$, hence to choose the averaging radius R_{av} . Although one can do that arbitrarily, we prefer to make use of all the information provided by the σ_i measurements. Therefore we choose $R_{\text{av}} = R_{25}$ for atomic gas, $R_{\text{av}} = \frac{1}{2}R_{25}$ for molecular gas and $R_{\text{av}} = R_{25}$ for stars, where R_{25} is the optical radius (B-band isophotal radius at 25 mag arcsec⁻²).

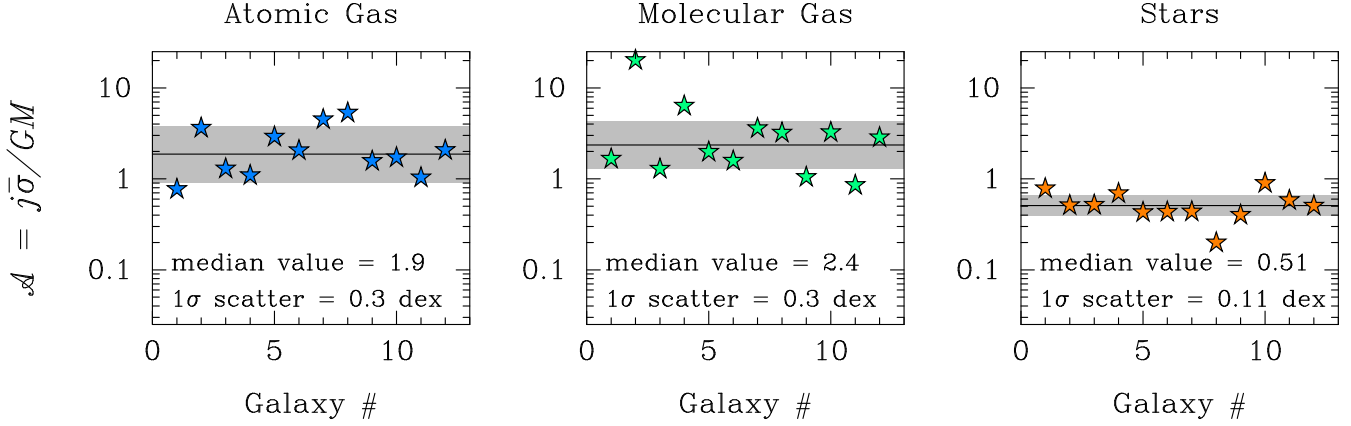


Figure 2. Galaxy-to-galaxy variation of the \mathcal{A} stability parameter for L08’s sample of spirals (the galaxy list is given in the first paragraph of Sect. 2.1). Also shown are the median value and 1σ scatter of \mathcal{A} .

In the case of molecular gas, the radial range is limited by the sparsity of sensitive CO measurements beyond half the optical radius (see fig. 1 of Romeo & Mogotsi 2017 and its discussion). Fig. 2 shows that the 1σ scatter of \mathcal{A}_i ranges from 0.1 dex, the value measured for stars, to 0.3 dex, the value measured for molecular and atomic gas. We have also carried out various tests, which show that the 1σ scatter of \mathcal{A}_i is unaffected by the choice of R_{av} , even if R_{av} is as small as $0.3 R_{25}$. Hereafter we will denote such galaxy-to-galaxy scatter with $\sigma_{\text{gg}}(i)$.¹

Before focusing on a more important meaning of σ_{gg} (see Sect. 2.3), let us test the robustness of the result $\sigma_{\text{gg}}(\star) < \sigma_{\text{gg}}(\text{gas})$ further. Is this an artifact of L08’s model-based $\sigma_{\star}(R)$? Current integral-field-unit (IFU) surveys allow measuring the mass-weighted average of $Q_{\star}(R)$ over the stellar half-light radius, R_{50} , but not beyond. This limit is imposed by the sparsity of reliable σ_{\star} measurements for $R \gtrsim R_{50}$ (Martinsson et al. 2013; Falc3n-Barroso et al. 2017; Mogotsi & Romeo 2019). Using radial profiles of σ_{\star} derived from CALIFA observations, Romeo & Mogotsi (2018) showed that $\sigma_{\text{gg}}(\star) \approx 0.2$ dex. This result is confirmed by an independent analysis that makes use of scaling relations (see again Romeo & Mogotsi 2018), and strengthens the conclusion that the galaxy-to-galaxy scatter of \mathcal{A}_i is smaller for stars (0.1–0.2 dex) than for molecular and atomic gas (0.3 dex).

2.3 Generating a new set of scaling relations

The small galaxy-to-galaxy scatter of \mathcal{A}_i means that the median of \mathcal{A}_i over the galaxy sample provides a reliable estimate of the value of \mathcal{A}_i in each galaxy: $\mathcal{A}_i \approx \mathcal{A}_{\text{med } i}$. This relation is more far-reaching than it looks. In fact, replacing \mathcal{A}_i with the right-hand side of Eq. (2) and dividing by $\mathcal{A}_{\text{med } i}$, we get:

$$\frac{j_i \hat{\sigma}_i}{GM_i} \approx 1, \quad (5)$$

¹ $\sigma_{\text{gg}}(i)$ can be combined with the total scatter given in Fig. 1, $\sigma_{\text{tot}}(i)$, to estimate the rms scatter of Q_i within a galaxy: $\sigma_{\text{g}}(i) = \sqrt{\sigma_{\text{tot}}^2(i) - \sigma_{\text{gg}}^2(i)}$. Hence $\sigma_{\text{g}}(\text{H1}) = 0.5$ dex, $\sigma_{\text{g}}(\text{H2}) = 0.2$ dex and $\sigma_{\text{g}}(\star) = 0.05$ dex.

Table 1. The atomic gas (H1), molecular gas (H2) and stellar (\star) C -factors appearing in Eq. (6) for various choices of the averaging radius (R_{av}), measured in units of either the stellar half-mass/light radius (R_{50}) or the B-band isophotal radius at 25 mag arcsec⁻² (R_{25}). In the case of molecular gas, the radial range is limited by the sparsity of sensitive CO measurements beyond half the optical radius.

R_{av}	C_{H1}	C_{H2}	C_{\star}
1.0 R_{50}	0.4	0.4	1.2
1.5 R_{50}	0.4	0.4	1.4
2.0 R_{50}	0.5	—	1.7
2.5 R_{50}	0.5	—	1.9
3.0 R_{50}	0.6	—	2.2
0.5 R_{25}	0.4	0.4	1.4
1.0 R_{25}	0.5	—	2.0

where $\hat{\sigma}_i \equiv \bar{\sigma}_i / \mathcal{A}_{\text{med } i}$. This is the *key* equation of our paper. It is not a marginal stability condition. It is instead a simple formula that one can use for generating new scaling relations, all driven by disc gravitational instability. For instance, multiply the left- and right-hand sides of Eq. (5) by M_i / M_{ref} , and you will get a set of scaling relations for the relative mass content of each component, where M_{ref} is any well-defined reference mass. Since each scaling relation is derived from Eq. (5) by multiplication, its (logarithmic) scatter will be identical to the scatter of Eq. (5), which itself is identical to the galaxy-to-galaxy scatter of the parent quantity \mathcal{A}_i . We will present the new set of scaling relations in Sect. 4. Here instead we go on explaining how to make use of Eq. (5).

- If reliable σ_i measurements are available, then one needs to know $C_i = 1 / \mathcal{A}_{\text{med } i}$. In our case $C_{\text{H1}} = 0.5$, $C_{\text{H2}} = 0.4$ and $C_{\star} = 2.0$ (see Fig. 2). But suppose that one chooses other values of the averaging radius R_{av} than those specified in Sect. 2.2, for instance because σ_i is measured only within the inner optical disc. In this case look at Table 1, where C_i is calibrated for various choices of R_{av} using L08’s sample of spirals, and compute $\hat{\sigma}_i$ as

$$\hat{\sigma}_i = C_i \bar{\sigma}_i, \quad (6)$$

where $\bar{\sigma}_i$ is given by Eq. (4).

• If reliable σ_i measurements are not available, then Eq. (5) is still valid provided that $\hat{\sigma}_i$ is redefined as $\hat{\sigma}_i \equiv (\bar{\sigma}/\mathcal{A})_{\text{med } i}$, the median of $\bar{\sigma}_i/\mathcal{A}_i$ over the galaxy sample. Once again, we calibrate this quantity using L08’s sample of spirals:

$$\hat{\sigma}_i = \begin{cases} 11 \text{ km s}^{-1} & \text{if } i = \text{H1}, \\ 8 \text{ km s}^{-1} & \text{if } i = \text{H2}, \\ 130 \text{ km s}^{-1} \times (M_*/10^{10.6} M_\odot)^{0.5} & \text{if } i = \star. \end{cases} \quad (7)$$

Note that *neither* in Eq. (6) *nor* in Eq. (7) we have assumed that $\sigma_i = \text{constant}$. In fact, as pointed out in Sects 1 and 2.1, we have used radial profiles of σ_i , and the resulting $\bar{\sigma}_i$ varies from galaxy to galaxy: for L08’s sample of spirals $\bar{\sigma}_{\text{H1}} \approx 9\text{--}31 \text{ km s}^{-1}$, $\bar{\sigma}_{\text{H2}} \approx 7\text{--}33 \text{ km s}^{-1}$ and $\bar{\sigma}_\star \approx 40\text{--}108 \text{ km s}^{-1}$. It is remarkable that the $\hat{\sigma}_{\text{H1}}$ and $\hat{\sigma}_{\text{H2}}$ specified in Eq. (7), in spite of being velocity dispersion scales based on mass and specific angular momentum [$\hat{\sigma}_i = (GM/j)_{\text{med } i}$], look like observationally motivated values of σ_{H1} and σ_{H2} . Note also that the $\hat{\sigma}_\star$ specified in Eq. (7) incorporates the approximate scaling $\bar{\sigma}_\star \propto M_\star^{0.5}$ (Gilhuly et al. 2019; Mogotsi & Romeo 2019), which is measured across spiral galaxies of type Sa–Sd and stellar mass $M_\star = 10^{9.5\text{--}11.5} M_\odot$. Finally, it may seem risky to calibrate C_i or $\hat{\sigma}_i$ using a single representative galaxy sample. However, to the best of our knowledge, L08’s sample is the only one that has reliable published measurements for all the quantities used in this analysis. We will test the robustness of our approach in Sect. 4.

3 GALAXY SAMPLES, DATA AND STATISTICS

To test the robustness of our approach and present the new set of scaling relations, we analyse 101 galaxies, from massive spirals to dwarf irregulars, spanning five orders of magnitude in M_\star , three and a half orders of magnitude in M_{H1} , and three orders of magnitude in M_{H2} . Such galaxies belong to five distinct samples, which we name and describe below together with the available data.

(i) ‘Sp (L08+)’ is the sample analysed in Sect. 2. It contains 12 spirals of type Sab–Sc from the THINGS, HERACLES and SINGS surveys. For these galaxies there are published measurements of M_{H1} , M_{H2} and M_\star (L08), j_{H1} , j_{H2} and j_\star (Obreschkow & Glazebrook 2014), σ_{H1} and σ_{H2} (Romeo & Mogotsi 2017), and σ_\star (L08).

(ii) ‘Sp (RM18+)’ contains 34 spirals of type Sa–Sd from the EDGE-CALIFA survey. For these galaxies there are published measurements of $\langle Q_\star \rangle_{50}$, the mass-weighted average of $Q_\star(R)$ over the stellar half-light radius (Romeo & Mogotsi 2018), σ_\star (Mogotsi & Romeo 2019), M_\star and M_{H2} (Bolatto et al. 2017). There is also a compilation of H I masses kindly provided by Alberto Bolatto and Tony Wong in advance of publication (the sources for the spectra are: van Driel et al. 2001; Springob et al. 2005; Courtois et al. 2009; Haynes et al. 2011; Masters et al. 2014; Wong et al., in preparation). For consistency with the analysis carried out in Sect. 2, we convert stellar masses from the Salpeter initial mass function (IMF) assumed by the CALIFA team (Cid Fernandes et al. 2013; Sánchez et al. 2016) to the Kroupa IMF assumed by L08, i.e. we divide M_\star and multiply $\langle Q_\star \rangle_{50}$ by 1.6. We then divide $\langle Q_\star \rangle_{50}$ by 3.6 to get \mathcal{A}_\star .

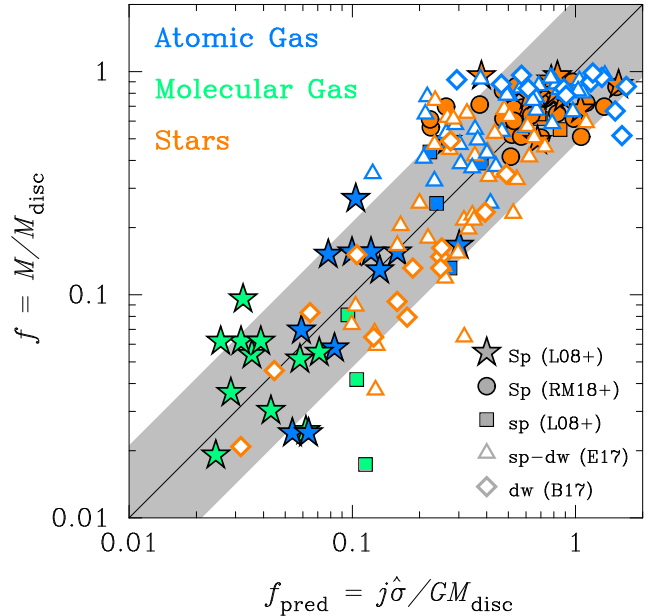


Figure 3. Measured (f) versus predicted (f_{pred}) mass fractions of atomic gas, molecular gas and stars for L08’s sample of spirals (star symbols), and for the other galaxy samples described in Sect. 3. Also shown are the predicted set of scaling relations, $f = j\hat{\sigma}/GM_{\text{disc}}$ (black line), and the predicted 1σ scatter, 0.23 dex (grey area). Note that 82% of the data points fall within the grey area, thus highlighting the accuracy of our prediction.

(iii) ‘sp (L08+)’ contains 4 small spirals of type Sc–Scd from the THINGS, HERACLES and SINGS surveys. For these galaxies there are published measurements of M_{H1} , M_{H2} and M_\star (L08), j_{H1} , j_{H2} and j_\star (Obreschkow & Glazebrook 2014), and σ_\star (L08).

(iv) ‘sp–dw (E17)’ contains 9 small late-type spirals and 28 dwarf irregulars from the WHISP survey. For these galaxies there are published measurements of M_{H1} , M_\star , j_{H1} and j_\star (Elson 2017).

(v) ‘dw (B17)’ contains 14 dwarf irregulars from the LITTLE THINGS survey. For these galaxies there are published measurements of M_{H1} , M_\star , j_{H1} and j_\star (Butler et al. 2017).

Note that for most of the galaxy samples there are no published measurements of σ_i , hence for those samples $\hat{\sigma}_i$ is computed from Eq. (7), as explained in Sect. 2.3. So, while we have shown that velocity dispersion plays an important role in our approach (see Sect. 2), we will not be able to quantify how significantly it affects the new set of scaling relations.

To quantify the tightness, strength and significance of the correlations between the quantities defining the new set of scaling relations, we present the results of several statistical measures and associated tests. First of all, we measure the dispersion of the data points around the predicted scaling relations using robust statistics: $\text{SD}_{\text{rob}} = 1/0.6745 \text{ MAD}$, where SD_{rob} is the robust counterpart of the standard deviation and MAD is the median absolute deviation (see, e.g., Müller 2000). Small values of SD_{rob} , for instance 0.2 dex, mean a tight correlation. Secondly, we measure Pearson’s r , Spearman’s ρ and Kendall’s τ correlation coefficients, together with their significance levels p_r , p_ρ and p_τ (see, e.g.,

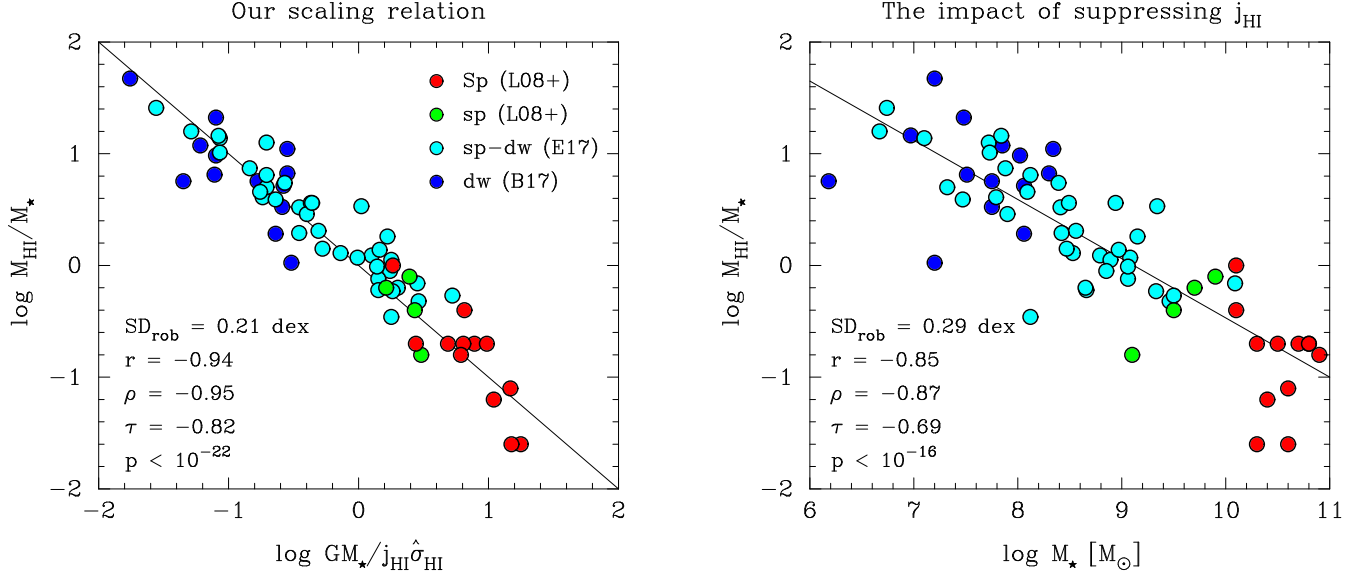


Figure 4. Our scaling relation for the relative mass content of atomic gas, and the impact of suppressing j_{HI} (this is the popular M_{HI}/M_* versus M_* scaling relation). Galaxy samples and statistics are denoted as in Sect. 3. The diagonal line in the left panel is the prediction based on disc gravitational instability, while the line in the right panel, $\log(M_{\text{HI}}/M_*) = -0.53 \log M_* + 4.83$, is a robust median-based fit to the data points.

Press et al. 1992). Values of $r, \rho, \tau \approx (-)1$ and $p_r, p_\rho, p_\tau \approx 0$ mean a strong and significant (anti)correlation.

4 THE NEW SET OF SCALING RELATIONS

4.1 The set as a whole

To give a first view of our scaling relations, we multiply Eq. (5) by $f_i = M_i/(M_{\text{HI}} + M_{\text{H}_2} + M_*)$, the mass fraction of component i . Although $M_{\text{HI}} + M_{\text{H}_2} + M_*$ is the total baryonic mass contained in the disc and in the (pseudo)bulge, we will simply denote it with M_{disc} since the sample galaxies are disc-dominated. The predicted scaling relations are then $f_i = j_i \hat{\sigma}_i / GM_{\text{disc}}$. Parametrizing in terms of f_i is not only natural and commonly used (e.g., Obreschkow et al. 2016; Lutz et al. 2017, 2018; Džudžar et al. 2019; Murugesan et al. 2019), but also useful for visualizing the new set of scaling relations as a whole, in a single plot.

Fig. 3 illustrates that this set stretches across two orders of magnitude in f_i , and applies not only to spirals of type Sa–Sd but also to dwarf irregulars. This is surprising, considering that such scaling relations have no free parameters and have been predicted analysing a single representative sample of spirals [Sp (L08+)]. Note also that the 1σ scatter measured for the whole galaxy sample is the same as the 1σ scatter measured for L08’s sample of spirals: $\text{SD}_{\text{rob}} = 0.23$ dex.

Despite being natural and useful, the f_i parametrization is not optimal. All massive spirals have $f_* \sim 1$, and all dwarf irregulars have $f_{\text{HI}} \sim 1$. This saturation does not influence the measurements of dispersion, which are entirely determined by the dispersion properties of the parent quantity \mathcal{A}_i (see Sect. 2.3), but may influence the measurements of correlation strength and significance. In view of that, it is important to test our scaling relations using other parametrizations. We do this in Sect. 4.2 for the cold gas scaling relation.

A detailed analysis of the stellar scaling relation is left for future work.

4.2 Scaling relation for the relative mass content of cold gas

To test our atomic gas scaling relation, we use another common parametrization: M_{HI}/M_* , the atomic gas-to-stellar mass ratio. Multiplying the $i = \text{HI}$ component of Eq. (5) by this quantity, we get the predicted scaling relation, $M_{\text{HI}}/M_* = j_{\text{HI}} \hat{\sigma}_{\text{HI}} / GM_*$, which can be rewritten as $\log(M_{\text{HI}}/M_*) = -\log(GM_*/j_{\text{HI}} \hat{\sigma}_{\text{HI}})$. Expressed in this form, our scaling relation can be directly compared with the popular $\log(M_{\text{HI}}/M_*)$ versus $\log M_*$ scaling relation, systematically studied by the teams of GASS (e.g., Catinella et al. 2010, 2012, 2018), ALFALFA (e.g., Huang et al. 2012; Papastergis et al. 2012), and other surveys (e.g., Cortese et al. 2011; Peebles & Shankar 2011). More importantly, such a comparison allows quantifying the impact of specific angular momentum on the atomic gas scaling relation. In fact, the dependence on velocity dispersion is nearly negligible: for all galaxy samples except one [Sp (L08+)], $\hat{\sigma}_{\text{HI}}$ is fixed (see Eq. 7) since there are no published measurements of σ_{HI} (see Sects 2.3 and 3). We have checked that fixing $\hat{\sigma}_{\text{HI}}$ even for Sp (L08+) leaves the statistical measurements unchanged.

Fig. 4 and the statistical measurements shown in the two panels illustrate that our scaling relation is more constrained than M_{HI}/M_* versus M_* . This may seem obvious because M_{HI}/M_* versus M_* is one of the gas scaling relations that have largest scatter (e.g., Catinella et al. 2018),² and because it has been demonstrated that M_{HI}/M_* versus

² The M_{HI}/M_* versus M_* relation presented here shows significantly less scatter than that presented by the GASS team (e.g., Catinella et al. 2018), who used a stellar mass-selected galaxy sample that is representative in terms of HI content. This mis-

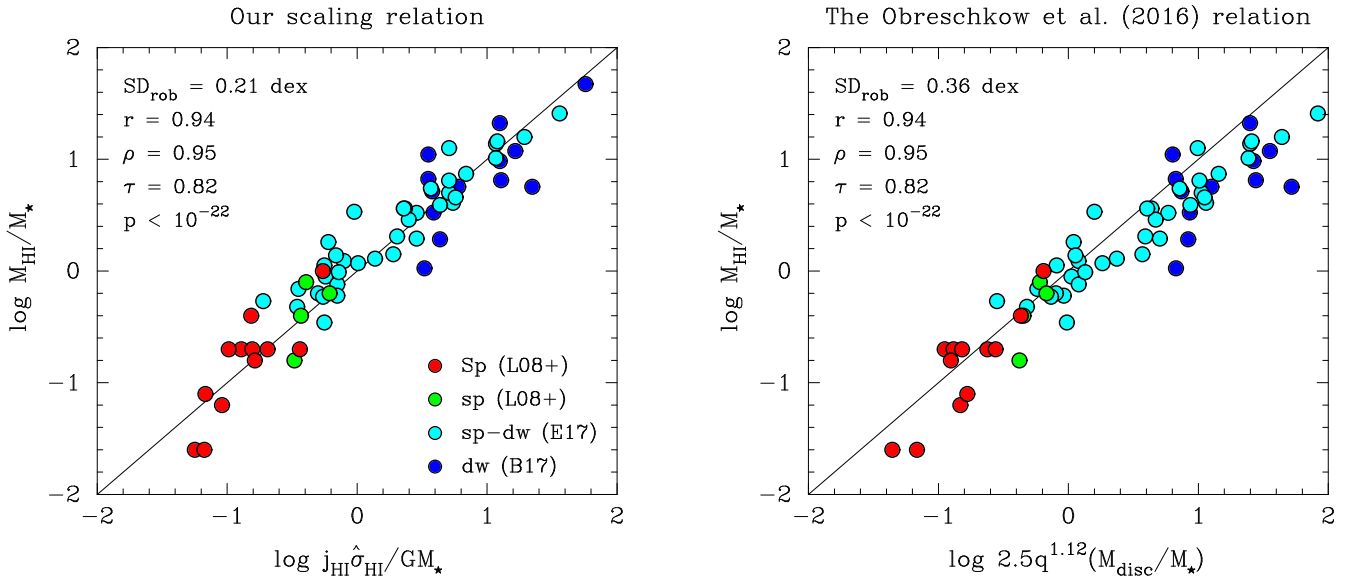


Figure 5. Comparison between our scaling relation for the relative mass content of atomic gas and the Obreschkow et al. (2016) scaling relation, where $q = j_{\text{disc}} \sigma_{\text{HI}} / GM_{\text{disc}}$ and $\sigma_{\text{HI}} = 10 \text{ km s}^{-1}$. Galaxy samples and statistics are denoted as in Sect. 3. The diagonal lines in the left and right panels are the two different predictions.

M_* is ‘not physical’ but driven by the relative fraction of star-forming and quiescent galaxies as a function of stellar mass (e.g., Brown et al. 2015). Note, however, that it is not at all obvious that a theoretical approach like ours, based on first principles and on a simple statistical analysis, succeeds in predicting both the slope and the zero-point of the atomic gas scaling relation across four orders of magnitude in M_{HI}/M_* , to within 0.2 dex, and without any free parameter or fine-tuning. These facts speak clearly. In particular, the small scatter of our scaling relation tells us that the mass-averaged gravitational instability properties of galaxy discs are remarkably uniform across the sequence Sa–dIrr, and that specific angular momentum has a significant impact on the atomic gas scaling relation.

A similar conclusion about specific angular momentum was drawn by Obreschkow et al. (2016), so it is interesting to compare our scaling relation with theirs: $f_{\text{HI}} = \min\{1, 2.5q^{1.12}\}$, where $q = j_{\text{disc}} \sigma_{\text{HI}} / GM_{\text{disc}}$ and $\sigma_{\text{HI}} = 10 \text{ km s}^{-1}$. To be precise, their stability model predicts that $f_{\text{HI}} = 2.5q^{1.12}$. The upper limit on f_{HI} was imposed to avoid mass ‘fractions’ $f_{\text{HI}} > 1$ for $q > 0.44$. Since this upper limit is not part of the prediction, we do not consider it. In addition, since the f_{HI} parametrization is open to the criticism pointed out in Sect. 4.1, we rewrite the Obreschkow et al. (2016) relation as $M_{\text{HI}}/M_* = 2.5q^{1.12}(M_{\text{disc}}/M_*)$, which can now be directly compared with ours: $M_{\text{HI}}/M_* = j_{\text{HI}} \hat{\sigma}_{\text{HI}} / GM_*$. Fig. 5 and the statistical measurements shown in the two panels illustrate that the Obreschkow et al. (2016) relation has the same correlation strength and significance as ours, but overpredicts M_{HI}/M_* in dwarf irregulars significantly,

match means that our galaxy sample, which is limited by the availability of accurate measurements of specific angular momentum, is not fully representative of the HI properties of the galaxy population in our stellar mass interval. Obviously, our work shares this limitation among all other works that have not used fully representative galaxy samples.

on average by 0.3 dex (a factor of 2). Our scaling relation does not show such a bias, and is thus a more reliable atomic gas tracer.

By analogy with the atomic gas case, our molecular gas scaling relation can be written as $\log(M_{\text{H}_2}/M_*) = -\log(GM_*/j_{\text{H}_2} \hat{\sigma}_{\text{H}_2})$. This scaling relation could, in principle, be directly compared with the popular $\log(M_{\text{H}_2}/M_*)$ versus $\log M_*$ scaling relation, systematically studied by the teams of COLD GASS (e.g., Saintonge et al. 2011, 2017), HRS (e.g., Boselli et al. 2014), and other surveys (e.g., Accurso et al. 2017; Gao et al. 2019; Liu et al. 2019). Unfortunately, as shown by Fig. 3 and confirmed by Danail Obreschkow (private communication), there is still a small number of published j_{H_2} measurements, too few to make a meaningful comparison. Note, however, that our molecular gas relation has the same expected scatter as our atomic gas relation (see Sect. 2), so we expect that it should also test well.

5 CONCLUSIONS

- Current models of star formation and/or galaxy evolution commonly assume that Toomre’s $Q \approx 1$. This assumption is not realistic enough to represent the diverse phenomenology of Q in galaxy discs (see Fig. 1). The data are now at the point where it is possible to do statistics, and look at how much variance there is in Q_{HI} , Q_{H_2} and Q_* , both from galaxy to galaxy and within a galaxy. The former type of variance is low for all the components, while the latter varies significantly not only from stars to gas but also between the molecular and atomic gas phases. The statistical measurements presented in this paper impose tight constraints on how self-regulated galaxy discs are, and will thus put new-generation models of star formation and/or galaxy evolution to a stringent test.

- The low galaxy-to-galaxy variance of Q_i results in a

simple formula (Eq. 5) that one can use for generating new scaling relations, all driven by disc gravitational instability. Eq. (5) is the key equation of our paper. We explain how to make use of it in Sect. 2.3.

- Making use of Eq. (5), we have generated a new set of scaling relations for the relative mass content of atomic gas, molecular gas and stars. We have analysed the set as a whole and each scaling relation using more than 100 galaxies, from massive spirals to dwarf irregulars, thus spanning five orders of magnitude in M_* and more than three orders of magnitude in M_{HI} . Such tests demonstrate that our scaling relations perform well (see Figs 3–5). In particular, our atomic gas–stellar mass relation is more physically motivated and has less scatter than the Obreschkow et al. (2016) relation (see Fig. 5). The performance of our scaling relations does not depend on any free parameter or fine-tuning, but results from our unified approach for cold gas and stars, which robustly predicts not only the scaling but also the zero-point of the relations.

- The tests carried out in this paper also demonstrate that the mass-averaged gravitational instability properties of galaxy discs are remarkably uniform across the sequence Sa–dIrr, and that specific angular momentum plays an important role in such a scenario (see Fig. 4). Velocity dispersion is another key quantity in our approach. However, limited by the sparsity of published velocity dispersion measurements, we have not been able to quantify how significantly it affects the new set of scaling relations.

Now that we have pointed out the strength of our approach, let us mention its weakness. Like all other approaches based on disc gravitational instability, our approach is calibrated/tested using ‘disc-dominated’ galaxies. While this concept is in common usage, observationally it is not well defined because it says little about the actual bulge mass fraction, B/T, which is an important ‘second parameter’. In view of that, one should test our scaling relations further, using a more complete galaxy sample and studying the outcome as a function of B/T. That test could show potential biases of our approach and suggest improvements. We leave that for future work.

Besides testing our scaling relations further, it would be exciting to generate new ones using Eq. (5). While in this paper we have chosen baryonic reference masses ($M_{\text{ref}} = M_{\text{disc}}, M_*$), one could parametrize the stellar scaling relation in terms of M_*/M_{halo} and compare it with the popular stellar-to-halo mass relation (e.g., Vale & Ostriker 2004; Dutton et al. 2010; Leauthaud et al. 2012; Behroozi et al. 2013; Moster et al. 2013; Rodríguez-Puebla et al. 2015; van Uitert et al. 2016; Posti et al. 2019). One could also parametrize in terms of j_*/j_{halo} and compare with the stellar-to-halo specific angular momentum relation (e.g., Dutton & van den Bosch 2012; Kauffmann et al. 2015; Posti et al. 2018b, 2019). We leave such exciting applications of Eq. (5) for future work.

ACKNOWLEDGEMENTS

We are very grateful to Alberto Bolatto and Tony Wong for providing us with a compilation of HI masses that they made for galaxies from the EDGE-CALIFA survey (see the references listed in item ii of Sect. 3), and to Ed Elson for

providing us with measurements of mass and specific angular momentum that he made for galaxies from the WHISP survey (Elson 2017). In addition, we are very grateful to Oscar Agertz, Alberto Bolatto, Françoise Combes, John Forbes, Mark Krumholz, Claudia Lagos, Lorenzo Posti and Florent Renaud for useful discussions. We are also very grateful to an anonymous referee for insightful comments and suggestions, for further constructive criticism and for encouraging future work on the topic.

REFERENCES

- Accurso G. et al., 2017, MNRAS, 470, 4750
 Agertz O., Kravtsov A. V., 2016, ApJ, 824, 79
 Agertz O. et al., 2019, preprint (arXiv:1904.02723)
 Athanassoula E., 2008, MNRAS, 390, L69
 Behroozi P. S., Wechsler R. H., Conroy C., 2013, ApJ, 770, 57
 Bertin G., 2014, Dynamics of Galaxies. Cambridge University Press, Cambridge
 Bigiel F., Blitz L., 2012, ApJ, 756, 183
 Binney J., Tremaine S., 2008, Galactic Dynamics. Princeton University Press, Princeton
 Bolatto A. D. et al., 2017, ApJ, 846, 159
 Boselli A., Cortese L., Boquien M., Boissier S., Catinella B., Lagos C., Saintonge A., 2014, A&A, 564, A66
 Bottema R., 1988, A&A, 197, 105
 Bottema R., 1993, A&A, 275, 16
 Brown T., Catinella B., Cortese L., Kilborn V., Haynes M. P., Giovanelli R., 2015, MNRAS, 452, 2479
 Butler K. M., Obreschkow D., Oh S.-H., 2017, ApJ, 834, L4
 Catinella B. et al., 2010, MNRAS, 403, 683
 Catinella B. et al., 2012, A&A, 544, A65
 Catinella B. et al., 2018, MNRAS, 476, 875
 Chowdhury A., Chengalur J. N., 2017, MNRAS, 467, 3856
 Cid Fernandes R. et al., 2013, A&A, 557, A86
 Cortese L., Catinella B., Boissier S., Boselli A., Heinis S., 2011, MNRAS, 415, 1797
 Courtois H. M., Tully R. B., Fisher J. R., Bonhomme N., Zavodny M., Barnes A., 2009, AJ, 138, 1938
 Dutton A. A., van den Bosch F. C., 2012, MNRAS, 421, 608
 Dutton A. A., Conroy C., van den Bosch F. C., Prada F., More S., 2010, MNRAS, 407, 2
 Dutton A. A. et al., 2011, MNRAS, 416, 322
 Džudžar R. et al., 2019, MNRAS, 483, 5409
 Efstathiou G., Lake G., Negroponte J., 1982, MNRAS, 199, 1069
 El-Badry et al., 2018, MNRAS, 473, 1930
 Elmegreen B. G., 2011, ApJ, 737, 10
 Elson E. C., 2017, MNRAS, 472, 4551
 Falcón-Barroso J. et al., 2017, A&A, 597, A48
 Fall S. M., Romanowsky A. J., 2018, ApJ, 868, 133
 Forbes J., Krumholz M., Burkert A., 2012, ApJ, 754, 48
 Forbes J. C., Krumholz M. R., Burkert A., Dekel A., 2014, MNRAS, 438, 1552
 Forbes J. C., Krumholz M. R., Speagle J. S., 2019, MNRAS, 487, 3581
 Ganda K., Falcón-Barroso J., Peletier R. F., Cappellari M., Em-sellem E., McDermid R. M., de Zeeuw P. T., Carollo C. M., 2006, MNRAS, 367, 46
 Gao Y. et al., 2019, preprint (arXiv:1911.02795)
 Gilhuly C., Courteau S., Sánchez S. F., 2019, MNRAS, 482, 1427
 Ginolfi M., Hunt L. K., Tortora C., Schneider R., Cresci G., 2019, preprint (arXiv:1907.06654)
 Griv E., Gedalin M., 2012, MNRAS, 422, 600
 Haynes M. P. et al., 2011, AJ, 142, 170
 Herrmann K. A., Ciardullo R., 2009, ApJ, 705, 1686

- Huang S., Haynes M. P., Giovanelli R., Brinchmann J., 2012, *ApJ*, 756, 113
- Kauffmann G., Huang M.-L., Moran S., Heckman T. M., 2015, *MNRAS*, 451, 878
- Krumholz M., Burkert A., 2010, *ApJ*, 724, 895
- Krumholz M. R., Burkert B., Forbes J. C., Crocker R. M., 2018, *MNRAS*, 477, 2716
- Kurapati S., Chengalur J. N., Pustilnik S., Kamphuis P., 2018, *MNRAS*, 479, 228
- Lagos C. d. P. et al., 2016, *MNRAS*, 459, 2632
- Lagos C. d. P., Theuns T., Stevens A. R. H., Cortese L., Padilla N. D., Davis T. A., Contreras S., Croton D., 2017, *MNRAS*, 464, 3850
- Leauthaud A. et al., 2012, *ApJ*, 744, 159
- Leroy A. K., Walter F., Brinks E., Bigiel F., de Blok W. J. G., Madore B., Thornley M. D., 2008, *AJ*, 136, 2782 (L08)
- Liu D. et al., 2019, preprint (arXiv:1910.12883)
- Lutz K. A. et al., 2017, *MNRAS*, 467, 1083
- Lutz K. A. et al., 2018, *MNRAS*, 476, 3744
- Marchuk A. A., 2018, *MNRAS*, 476, 3591
- Marchuk A. A., Sotnikova N. Y., 2018, *MNRAS*, 475, 4891
- Martinsson T. P. K., Verheijen M. A. W., Westfall K. B., Ber-shady M. A., Schechtman-Rook A., Andersen D. R., Swaters R. A., 2013, *A&A*, 557, A130
- Masters K. L., Crook A., Hong T., Jarrett T. H., Koribalski B. S., Macri L., Springob C. M., Staveley-Smith L., 2014, *MNRAS*, 443, 1044
- Mo H. J., Mao S., White S. D. M., 1998, *MNRAS*, 295, 319
- Mogotsi K. M., Romeo A. B., 2019, *MNRAS*, 489, 3797
- Moster B. P., Naab T., White S. D. M., 2013, *MNRAS*, 428, 3121
- Müller J. W., 2000, *J. Res. Natl. Inst. Stand. Technol.*, 105, 551
- Murugesan C., Kilborn V., Obreschkow D., Glazebrook K., Lutz K., Džudžar R., Dénes H., 2019, *MNRAS*, 483, 2398
- Obreschkow D., Glazebrook K., 2014, *ApJ*, 784, 26
- Obreschkow D. et al., 2015, *ApJ*, 815, 97
- Obreschkow D., Glazebrook K., Kilborn V., Lutz K., 2016, *ApJ*, 824, L26
- Okamura T., Shimasaku K., Kawamata R., 2018, *ApJ*, 854, 22
- Papastergis E., Cattaneo A., Huang S., Giovanelli R., Haynes M. P., 2012, *ApJ*, 759, 138
- Peebles M. S., Shankar F., 2011, *MNRAS*, 417, 2962
- Posti L., Fraternali F., Di Teodoro E. M., Pezzulli G., 2018a, *A&A*, 612, L6
- Posti L., Pezzulli G., Fraternali F., Di Teodoro E. M., 2018b, *MNRAS*, 475, 232
- Posti L., Marasco A., Fraternali F., Famaey B., 2019, *A&A*, 629, A59
- Press W. H., Teukolsky S. A., Vetterling W. T., Flannery B. P., 1992, *Numerical Recipes in Fortran: The Art of Scientific Computing*. Cambridge University Press, Cambridge
- Renaud F., 2019, preprint (arXiv:1908.02301)
- Rodríguez-Puebla A., Avila-Reese V., Yang X., Foucaud S., Drory N., Jing Y. P., 2015, *ApJ*, 799, 130
- Romeo A. B., Agertz O., 2014, *MNRAS*, 442, 1230
- Romeo A. B., Falstad N., 2013, *MNRAS*, 433, 1389
- Romeo A. B., Fathi K., 2015, *MNRAS*, 451, 3107
- Romeo A. B., Fathi K., 2016, *MNRAS*, 460, 2360
- Romeo A. B., Mogotsi K. M., 2017, *MNRAS*, 469, 286
- Romeo A. B., Mogotsi K. M., 2018, *MNRAS*, 480, L23
- Romeo A. B., Burkert A., Agertz O., 2010, *MNRAS*, 407, 1223
- Saintonge A. et al., 2011, *MNRAS*, 415, 32
- Saintonge A. et al., 2017, *ApJS*, 233, 22
- Sánchez S. F. et al., 2016, *Rev. Mex. Astron. Astrofis.*, 52, 171
- Sellwood J. A., 2016, *ApJ*, 819, 92
- Springob C. M., Haynes M. P., Giovanelli R., Kent B. R., 2005, *ApJS*, 160, 149
- Stevens A. R. H., Croton D. J., Mutch S. J., 2016, *MNRAS*, 461, 859
- Stevens A. R. H., Lagos C. d. P., Obreschkow D., Sinha M., 2018, *MNRAS*, 481, 5543
- Stevens A. R. H. et al., 2019, *MNRAS*, 483, 5334
- Sweet S. M. et al., 2019, *MNRAS*, 485, 5700
- Swinbank A. M. et al., 2017, *MNRAS*, 467, 3140
- Toomre A., 1964, *ApJ*, 139, 1217
- Vale A., Ostriker J. P., 2004, *MNRAS*, 353, 189
- Valencia-Enríquez D., Puerari I., Rodrigues I., 2019, *AJ*, 157, 175
- van Driel W., Marcum P., Gallagher III J. S., Wilcots E., Guidoux C., Monnier Ragaïgne D., 2001, *A&A*, 378, 370
- van Uiter E. et al., 2016, *MNRAS*, 459, 3251
- Wang L. et al., 2018, *ApJ*, 868, 93
- Wong T. et al., in preparation
- Zasov A. V., Zaitseva N. A., 2017, *Astron. Lett.*, 43, 439
- Zoldan A., De Lucia G., Xie L., Fontanot F., Hirschmann M., 2018, *MNRAS*, 481, 1376

This paper has been typeset from a \TeX / \LaTeX file prepared by the author.